Journal of Power Sources 220 (2012) 377–382

Contents lists available at SciVerse ScienceDirect

Journal of Power Sources

journal homepage: www.elsevier.com/locate/jpowsour

Electrochemical properties of ceria-based intermediate temperature solid oxide fuel cell using microwave heat-treated $La_{0.1}Sr_{0.9}Co_{0.8}Fe_{0.2}O_{3-\delta}$ as a cathode

M.-B. Choi [a], K.-T. Lee [b], H.-S. Yoon [b], S.-Y. Jeon [a], E.D. Wachsman [b], S.-J. Song [a,*]

[a] Department of Materials Science and Engineering, Chonnam National University, 300 Yongbong-dong, Buk-gu, Gwangju 500-757, South Korea
[b] Department of Materials Science and Engineering, University of Maryland, College Park, MD 20742, USA

HIGHLIGHTS

- New promising cathode material of IT-SOFC was suggested.
- Cathode microstructure effects by microwave heating were reported.
- OCP and maximum power density were respectively 0.753 V and 1.79 W cm^{-2} at 650 °C.

GRAPHICAL ABSTRACT

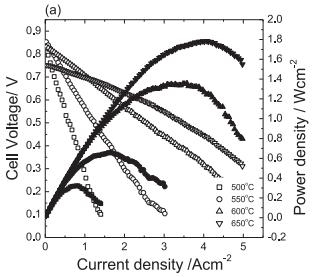

ARTICLE INFO

Article history:
Received 31 May 2012
Received in revised form
19 June 2012
Accepted 31 July 2012
Available online 9 August 2012

Keywords:
IT-SOFC
Cathode
Chemical diffusion coefficient
Surface exchange coefficient
Microwave sintering

ABSTRACT

The temperature dependence of the chemical diffusion coefficient and the surface exchange coefficient of LSCF1982 is successfully determined from the D.C. conductivity relaxation in the temperature range of $500 \leq T/°C \leq 700$ and an oxygen partial pressure of 0.21 atm. The kinetic values of chemical diffusion coefficient ($\tilde{D}$) and surface exchange coefficient (k) are 1.85×10^{-5} cm^2 s^{-1} and 2.42×10^{-4} cm s^{-1} at 650 °C, respectively. The electrochemical properties of $La_{0.1}Sr_{0.9}Co_{0.8}Fe_{0.2}O_{3-\delta}$ (LSCF1982) as a cathode for ceria based IT-SOFC are successfully characterized by I–V performance measurement and electrochemical impedance spectroscopy (EIS) in terms of cathode microstructure effects by using microwave heat treatment. The cell with microwave heat-treated cathode shows the higher performance than conventional heat treated cathode. At 650 °C the open circuit potential (OCP) and maximum power density are respectively 0.753 V and 1.79 W cm^{-2} under 150 sccm of wet hydrogen and air gas flow conditions, and the ohmic and electrode area specific resistance (ASR) are 0.037 and 0.014 Ω cm^2, respectively.

1. Introduction

Solid oxide fuel cells (SOFCs) are devices that generate electricity and heat by electrochemical reaction and are known as eco-friendly devices with higher efficiency than the conventional methods for electricity production. SOFCs using YSZ electrolyte are generally reported to operate at a higher temperature of about 1000 °C [1–3]. They have rapid electrodes kinetics without the use of noble metal electrode and can use the hydrocarbons as fuel. Furthermore, the heat produced while operating an SOFC system can be used in various applications. However, they have disadvantages such as cell degradation and higher cost for durability because of operation at high temperature [4,5]. Therefore, many studies are now focused on the development of intermediate-temperature SOFCs (IT-SOFC; 600–800 °C) to overcome these problems caused by high operating temperature. As a result, the long term stability and the cost-effectiveness for durability are improved by lowering the operating temperature. However, this

* Corresponding author. Tel.: +1 82 62 530 1706; fax: +1 82 62 530 1699.
E-mail address: song@chonnam.ac.kr (S.-J. Song).

0378-7753/$ – see front matter © 2012 Elsevier B.V. All rights reserved.
http://dx.doi.org/10.1016/j.jpowsour.2012.07.122

decreases the electrochemical performance of the SOFC electrodes, because the electrode kinetics and transports are mostly thermally activated processes. Therefore, one major issue in IT-SOFC research is the development of cathode electrode materials [6,7].

ABO_3 perovskite structure-type mixed-ionic-electronic conducting (MIEC) oxides are one candidate materials for IT-SOFC cathodes because of their superior performance compared to other structure-type MIEC oxides, which is directly attributed to the partial substitution of both A and B-site cations in the structure and its effect on accelerating the generation of oxygen vacancies via defect reaction [8–10].

Recently, $La_{0.1}Sr_{0.9}Co_{0.8}Fe_{0.2}O_{3-\delta}$ (LSCF1982) [11,12] was reported as an excellent surface catalyst. Its higher catalytic effect can be explained by previously reported quantitative defect analysis and fundamental properties, including oxygen nonstoichiometry, ionic conductivity, chemical diffusion coefficient and surface exchange coefficient, which were successfully derived in our previous work by coulometric titration, oxygen permeability study and four-probe D.C. conductivity relaxation method. It has a high concentration of oxygen vacancies, and shows nearly ~1 Scm^{-1} ionic conductivity at 800 °C in air atmosphere [13,14]. And also, it has a higher chemical diffusion coefficient and surface exchange coefficient than the general MIEC oxides above 800 °C. Therefore, LSCF1982 can be applied to SOFC cathodes. In the present work, the chemical diffusion coefficient and surface exchange coefficient were estimated by four-probe D.C. conductivity relaxation method in the intermediate temperature range. Anode supported button cells were fabricated by tape casting and dip coating method. The LSCF1982 cathode layer was coated by screen print method and heat treated by two methods – conventional thermal heat treatment and microwave heat treatment, to evaluate the structure effect for the cell performance. The electrochemical properties of LSCF1982 as a cathode for ceria based IT-SOFC were characterized by I–V performance measurement and electrochemical impedance spectroscopy (EIS) in various intermediate temperatures.

2. Experimental

Mixed oxygen ion-electron conducting LSCF1982 powders were prepared by solid state reaction method. The starting materials were La_2O_3 (Alfa aesar, 99.9%), $SrCO_3$ (Alfa aesar, 99.9%), Co_3O_4 (Alfa aesar, 99.9%), and Fe_2O_3 (Alfa aesar, 99.99%). The weighted stoichiometry amounts of the components were ball-milled for 24 h with ethanol solvent and calcined at 1000 °C for 12 h in air. The calcined powder was then planetary ball-milled with stabilized zirconia balls for 4 h at 320 rpm.

The obtained powder was mono-axially pressed, than cold isostatically pressed at 150 MPa. The obtained green pallets were sintered at 1200 °C in air for 10 h. The dense specimens (theoretical density ~95%) were for four-probe D.C. conductivity relaxation measurements were prepared as rectangular bars with 1.25 × 1.25 × 15.8 mm dimensions. The measurement was conducted using a Labview control system consisting of a programmable current source (Keithley 220) and digital multimeter (Keithley 2700) [13]. For the four-probe D.C. conductivity relaxation measurements, a specimen was completely equilibrated in a given thermodynamic condition and then the oxygen chemical potential was abruptly changed to a different value while recording the specimen's electrical conductivity vs. time until a new equilibrium was reached. In order to regard the chemical diffusivity as constant, a sufficiently small change of OPP was chosen. The chemical diffusion and surface exchange coefficients were extracted from the four-probe D.C. conductivity relaxation profile at the various intermediate temperatures ($500 \leq T/°C \leq 700$).

NiO-GDC10 anode support substrates were prepared by tape casting method [15,16]. The mixture slurry of NiO (Kceracell; BET = 4–6 $m^2\ g^{-1}$, d50 = 0.3–0.6 μm) and $Ce_{0.9}Gd_{0.1}O_{1.95}$ (Kceracell; BET = 5–8 $m^2\ g^{-1}$, d50 = 0.3–0.5 μm) was prepared in two steps. Firstly, NiO and $Ce_{0.9}Gd_{0.1}O_{1.95}$ (GDC10) powders were dispersed with fish oil (Aldrich) as a dispersant in a binary solvent (toluene:ethanol = 1:1 wt%) system for 24 h by ball-mill. Then, butyl benzyl phthalate (BBP), polyethylene glycol (PEG) were added as plasticizer and polyvinyl butyral (PVB) was added as binder, and ball milled for 24 h. A de-airing process was conducted to prevent defects caused by air bubbles in the slurry. NiO-GDC10 anode support tapes were fabricated by a tape casting process, and 25 mm diameter circles were punched from the obtained green sheet (thickness; about 350 μm) for the button cell test. Finally, the cut anode tapes were partially sintered at 900 °C for 2 h.

A NiO-GDC10 anode functional layer (AFL) was applied on the anode support by dip coating method. The AFL coating slurry of NiO (Kceracell; BET = 8–12 $m^2\ g^{-1}$, d50 = 0.2–0.5 μm)-GDC10 (Kceracell/BET = 5–8 $m^2\ g^{-1}$, d50 = 0.3–0.5 μm) was prepared in an ethanol based solvent [17]. Then, AFL coated samples were heat-treated at 400 °C for 2 h to burn out the organic materials present in the coating slurry. GDC10 electrolyte was coated onto the prepared AFL coated sample by dip coating method. The electrolyte coating slurry of GDC10 (Kceracell/BET = 10–15 $m^2\ g^{-1}$, d50 = 0.3–0.6 μm) was also prepared in an ethanol based solvent [17]. Then, the above samples were fully sintered at 1450 °C for 5 h in air atmosphere. The linear shrinkage rate of the sintered button cell was about 20%.

LSCF1982 paste was prepared using a planetary centrifugal mixer (Thinky, AR-100) with vehicle (ESL, type-441) to evaluate the electrochemical characteristics for application as an IT-SOFC cathode. Then, the LSCF1982 cathode layer was coated onto the as-prepared button cell by screen printing method. The area of the cathode layer was about 0.5 cm^2. In order to study the effect of heat treatment condition on the structure of cathode layer, two button

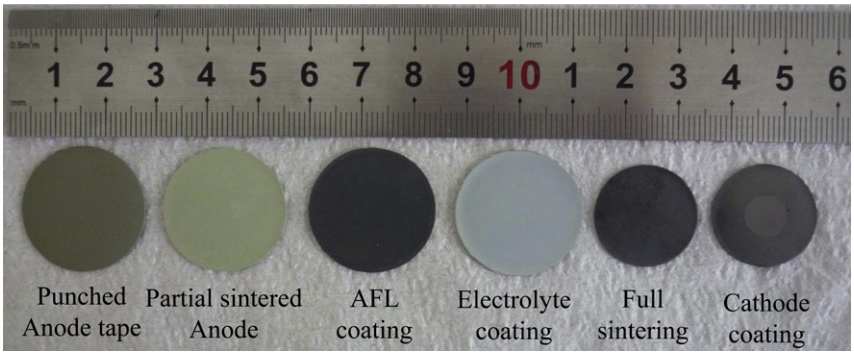

Fig. 1. Image of button cell fabrication procedure, which consisted of Ni-GDC10 anode support, Ni-GDC10 AFL, GDC10 electrolyte and LSCF1982 cathode.

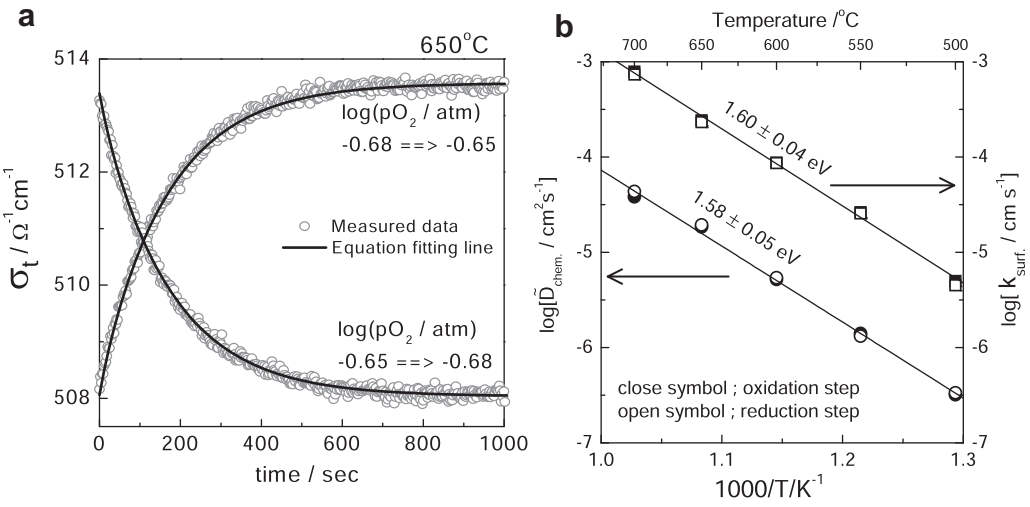

Fig. 2. (a) Typical D.C. conductivity relaxation profile of LSCF1982 at 650 °C (b) temperature dependence of the chemical diffusion coefficient and surface exchange coefficient of LSCF1982 under air atmosphere.

cells were separately heat-treated by microwave furnace (950 °C for 2 min.) and conventional electric furnace (1100 °C for 1 h.). The overall procedure of button cell fabrication is presented in the Fig. 1.

The button cell performance was evaluated at different temperatures ($500 \leq T/°C \leq 650$) and gas flow rates using a lab-made test system. The fuel side was sealed with a high temperature ceramic adhesive (Aremco Ceramabond™ 571). Silver mesh was used as a current collector for both the cathode and anode. Two Pt wires connected to the each sides of silver mesh were used as voltage and current probes, respectively. I–V measurements with scan rate of 0.05 A cm^{-2} and electrochemical impedance spectroscopy (EIS) were carried out under open circuit condition using a potentiostat (Reference 3000, Gamry Instruments) over a frequency range of 100 mHz–1 MHz with ac signal strength of 20 mV.

3. Results and discussion

Fig. 2(a) shows the typical conductivity relaxation profiles of the mean total conductivity upon oxidation and reduction across an identical oxygen activity window. The time dependent transient behavior in the equilibrium process can be best-fitted with Fick's second law [13,18].

$$\frac{\overline{\sigma}(t)-\sigma(0)}{\sigma(\infty)-\sigma(0)} = 1 - \left[\sum_{n=1}^{\infty} \frac{2(\beta_n \tan\beta_n)^2 \exp\left(-\frac{\beta_n^2 \tilde{D}(t-t_0)}{a^2}\right)}{\beta_n^2\left(\beta_n^2 + (\beta_n\tan\beta_n)^2 + \beta_n\tan\beta_n\right)}\right]^2 \quad (1)$$

where β_n is the positive root of

$$\beta_n \tan\beta_n = L, \quad L = \frac{ak}{\tilde{D}} \quad (2)$$

where $\sigma(0)$ and $\sigma(\infty)$ denote the equilibrium total conductivity before ($t = 0$) and after the relaxation ($t = \infty$), respectively, t is the time, k is the surface reaction rate constant, and $\tilde{D}$ is the chemical-diffusion coefficient. The chemical diffusion coefficient and surface reaction rate constant were determined by non-linear-least-square equation fitting of Eq. (1) for the relaxation data in Fig. 2(a). The temperature dependence of the chemical diffusion coefficient and the surface exchange coefficient of LSCF1982 obtained from the D.C. conductivity relaxation in the temperature range of $500 \leq T/°C \leq 700$ and in an oxygen partial pressure of 0.21 atm are shown in Fig. 2(b). The determined chemical

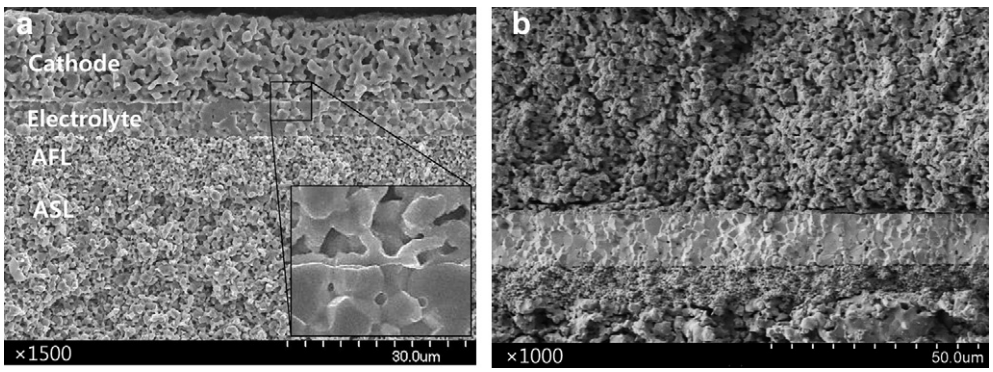

Fig. 3. SEM micrograph of button cell, (a) cathode LSCF1982 which was heat-treated at 950 °C by microwave furnace, (b) cathode LSCF1982 which was heat-treated at 1100 °C by electric furnace.

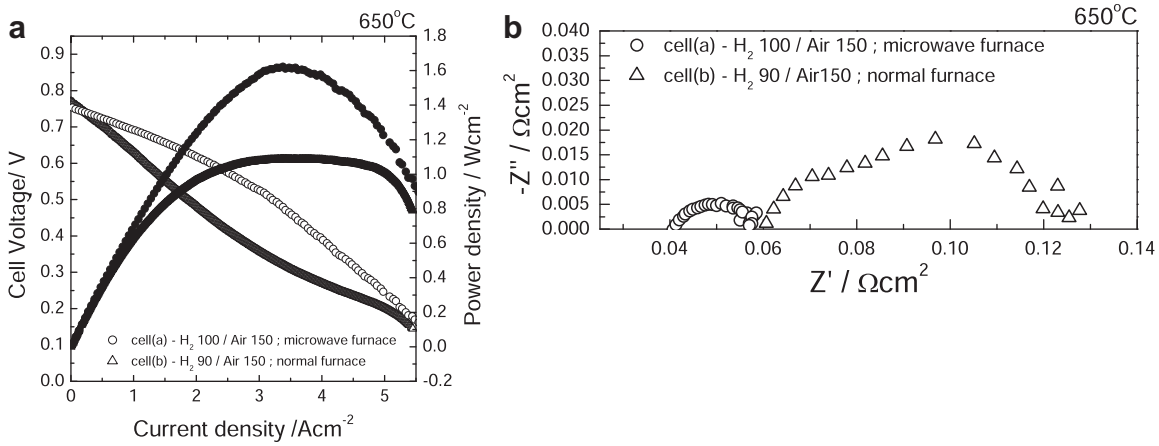

Fig. 4. The structure effect of cathode for the cell performance at 650 °C, (a) I–V tests of button cell at 650 °C, (b) EIS of button cell at 650 °C under the open circuit condition.

diffusion coefficient and surface exchange coefficient of LSCF1982 show higher values than the others cathode materials generally used in IT-SOFC. The kinetic values of $\tilde{D}$ and k were 1.85×10^{-5} cm^2 s^{-1} and 2.42×10^{-4} cm s^{-1} at 650 °C, respectively. The Arrhenius type of $\tilde{D}$ and k as functions of reciprocal temperature are best shown as

$$\tilde{D}/\mathrm{cm}^2\ \mathrm{s}^{-1} = 3.42 \times 10^3 \exp\left(-\frac{1.58 \pm 0.05\mathrm{eV}}{kT}\right)\Big|_{pO_2=0.21\ \mathrm{atm}}$$

$$k/\mathrm{cm}\ \mathrm{s}^{-1} = 1.55 \times 10^5 \exp\left(-\frac{1.60 \pm 0.04\mathrm{eV}}{kT}\right)\Big|_{pO_2=0.21\ \mathrm{atm}}$$

The surface exchange kinetics was an order of magnitude faster than the bulk diffusion. These higher kinetics properties at intermediate temperatures support that LSCF1982 is a promising candidate for cathode in the IT-SOFCs.

Fig. 3 shows the scanning electron micrograph (SEM) of a cross-section of the button cell assembly consisting of Ni-GDC10 anode support, Ni-GDC10 AFL, GDC10 electrolyte and LSCF1982 cathode which was respectively heat treated by microwave furnace (cell(a)) normal electric furnace (cell(b)). Fig. 3 shows that both of the Ni-GDC10 anode substrate and functional layer are sufficiently porous for gas diffusion, and GDC10 electrolyte is highly dense and is without the open pores. On the other hand, Fig. 3 shows that the cathode layer of cell(a) has more open structure, smaller grain size and good state of adhesion between the LSCF1982 cathode and the electrolyte than that in cell(b).

Fig. 4(a) shows the effect of heat treatment method of cathode on I–V cell performance that was respectively measured under the 150 sccm air/100 sccm hydrogen and 150 sccm air/90 sccm hydrogen gas flow condition at 650 °C. The open circuit potential (OCP) of cell(a) was slightly lower than cell(b), because cell(a) has a thin electrolyte than cell(b), as shown in Fig. 3. However, the maximum power densities were measured to be 1.62 W cm^{-2} and 1.07 W cm^{-2} respectively for cell(a) and cell(b). Although the fuel cell measurement conditions were different for two cells, the maximum power density of cell(a) was higher than cell(b). The EIS of cell(a) and cell(b) is shown in Fig. 4(b) and the calculated values of electrode area specific resistance (ASR) from EIS were 0.017 Ω cm^2 and 0.064 Ω cm^2, respectively. We believe that the higher performance and the low electrode ASR of cell(a) is mainly determined by the structure of cathode layer which has a more open pore, lower grain size and good adhesion to the electrolyte, as

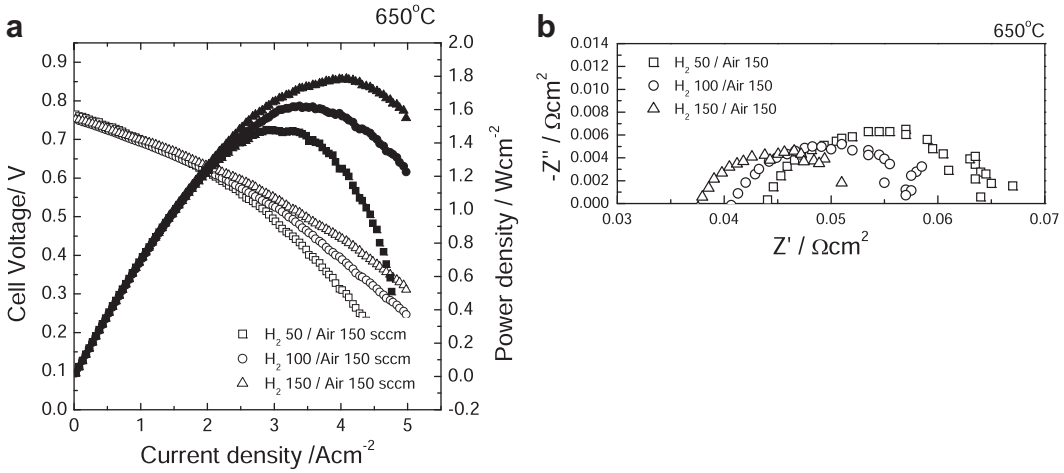

Fig. 5. The effect of hydrogen gas flow rate on cell performance at 650 °C, (a) I–V tests of button cell as a function of hydrogen gas flow rate at 650 °C, (b) EIS of button cell at 650 °C under the open circuit condition.

Table 1
Total, electrode and ohmic ASR as a function wet-hydrogen gas flow rate that were calculated from I–V curve and EIS at 650 °C.

Gas flow rate/ sccm	Total ASR_{IV}/ Ω cm^2	Total ASR_{EIS}/ Ω cm^2	$ASR_{Electrode}$/ Ω cm^2	ASR_{Ohmic}/ Ω cm^2
50	0.062	0.065	0.021	0.044
100	0.059	0.058	0.017	0.041
150	0.046	0.051	0.014	0.037

compared to cell(b). The difference of cathode structure can be explained by the "microwave effect". In microwave heating the energy is directly transferred to the material through molecular interaction and, therefore, it has several beneficial effects, including rapid volumetric heating, shorter sintering times, lower sintering temperatures, selective heating, and an additional driving force for diffusion mechanism compared to conventional thermal processing [19].

Fig. 5(a) shows the results of I–V tests of cell(a) that were measured as a function of hydrogen gas flow rate under a fixed air flow rate of 150 sccm at 650 °C. During the measurements the hydrogen gas was used in wet-state (3% $H_2O_{(g)}$). Under the 150 sccm of wet hydrogen and air gas flow condition, OCP and maximum power density were 0.753 V and 1.79 W cm^{-2} respectively. The power density was enhanced with the increasing wet-hydrogen gas flow, because concentration polarization was overcome. However, despite the concentration polarization, the power density was recorded to have a value (1.48 W cm^{-2}) in the 50 sccm hydrogen gas flow condition. The total ASR_{I-V} was estimated from the initial slope of the I–V curve, and it was reported to be 0.062 Ω cm^2, 0.059 Ω cm^2 and 0.046 Ω cm^2 with the increasing hydrogen gas flow. These values are lower than general ASR of IT-SOFCs that combine GDC electrolyte with LSCF-GDC composite cathodes. This high cell performance intensively supports that LSCF1982 is a promising material for IT-SOFC cathodes and the low electrode ASR value, shown in Fig. 5(b), is an evidence of this. The calculated values of ASR from EIS and I–V curve are given in Table 1. Table 1 shows the reduction of total and electrode ASR of the button cell with the increase in hydrogen gas flow. The reduction in ohmic ASR is due to the electron transfer, because GDC10 has a narrow electrolytic domain and thin electrolyte thickness, as shown in Fig. 3 [20]. Therefore, the OCP is also decreased accordingly with the increase in hydrogen gas flow.

The cell voltage and power density as a function of current density at various temperature from 500 °C to 650 °C are given in Fig. 6(a). During the experiment, 150 sccm wet hydrogen and dry air gas were constantly supplied. The OCPs/maximum power densities were measured to be 0.753 V/1.79 W cm^{-2}, 0.840 V/1.35 W cm^{-2}, 0.863 V/0.65 W cm^{-2} and 0.836 V/0.32 W cm^{-2} at 650, 600, 550 and 500 °C, respectively. Generally, the cell voltage was dropped with the increasing temperature and current density, and the maximum power densities were enhanced with the increasing temperature, because its overall kinetics is a thermally activated process. Fig. 6(b) shows the EIS at various temperatures from 500 °C to 650 °C under the open circuit condition. The ohmic and electrode ASR are derived from the impedance arcs. The ohmic ASR is defined from the intercept of the impedance arc at the real axis in the range of high frequency, and the electrode ASR is calculated from the diameter of the impedance arc. The values of ohmic, electrode, and total ASR are shown in the Fig. 6(c). The total ASR from EIS and I–V tests has similar values and increase with decreasing temperature. The activation energies for ohmic and electrode ASR were 0.63 eV and 1.34 eV, respectively. At 650 °C the values of electrode ASR is lower than the ohmic ASR. However, with the decrease in temperature the electrode ASR is increased and has a higher value than ohmic ASR, which indicates that the dependency of overall kinetics was changed from ohmic polarization to electrode polarization with the decreasing temperature.

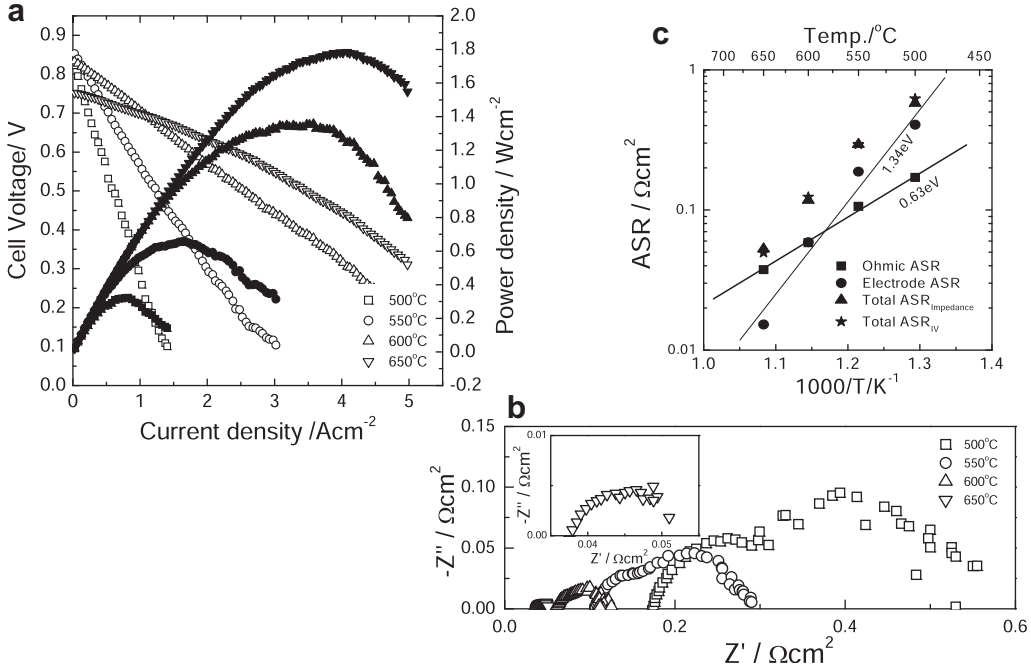

Fig. 6. Electrochemical properties of button cell as a function of temperatures, (a) performance of button cell as a function of temperatures under 150 sccm wet hydrogen and air gas, (b) EIS of button cell at the various temperatures, (c) several ASR as a function of temperature.

4. Conclusions

The temperature dependence of the chemical diffusion coefficient and the surface exchange coefficient of LSCF1982 was successfully determined from the D.C. conductivity relaxation in the temperature range of $500 \leq T/^{\circ}C \leq 700$ and an oxygen partial pressure of 0.21 atm. The kinetic values of $\tilde{D}$ and k were 1.85×10^{-5} cm^2 s^{-1} and 2.42×10^{-4} cm s^{-1} at 650 °C, respectively. These higher kinetics properties at intermediate temperatures intensively support that LSCF1982 is a promising material for IT-SOFC cathodes.

An anode supported ceria based button cell was successfully fabricated by tape casting and dip coating methods. The screen printing method was used to coat the cathode layer of synthesized LSCF982 onto the fabricated button cell. The electrochemical properties of LSCF1982 as a cathode of IT-SOFC were successfully characterized using I–V cell performance test and EIS. The effect of cathode microstructure on the cell performance was evaluated by using button cells having microwave furnace heat-treated cathode and conventionally heat-treated cathode. The cell with microwave heat-treated cathode layer shows the higher performance than conventional heat treated cathode. For the button cell with the microwave heat-treated cathode, the OCP and maximum power density, at 650 °C under 150 sccm of wet hydrogen and air flow conditions, were 0.753 V and 1.79 W cm^{-2} respectively and the ohmic and electrode ASR were 0.037 and 0.014 Ω cm^2, respectively. The maximum power densities were decreased with decreasing temperature and hydrogen gas flow rate. The activation energies for ohmic and electrode ASR were 0.63 eV and 1.34 eV, respectively. At 650 °C the electrode ASR was lower than the ohmic ASR. However, the electrode ASR was increased with the decrease in temperature and took a higher value than the ohmic ASR, indicating that the dependency of overall kinetics was changed from ohmic polarization to electrode polarization with decrease in temperature.

Acknowledgment

This work was supported by Solid Oxide Fuel Cell of Mew & Renewable Energy R&D Program (20093021030010) under the Korea Ministry of Knowledge Economy (MIKE)

References

[1] S.C. Singhal, Solid State Ionics 135 (2000) 305–313.
[2] S. Mcintosh, R.J. Gorte, Chem. Rev. 104 (2004) 4845–4865.
[3] S.M. Haile, Acta Mater. 51 (2003) 5981–6000.
[4] B.C.H. Steele, Solid State Ionics 134 (2000) 3–20.
[5] B.C.H. Steele, J. Power Sources 49 (1994) 1–14.
[6] J. Richter, P. Holtappels, T. Graule, T. Nakamura, L.J. Gauckler, Monatsh. Chem. 140 (2009) 985–999.
[7] E.D. Wachsman, K.-T. Lee, Science 334 (2011) 935–939.
[8] L.W. Tai, M.M. Nasrallah, H.U. Anderson, D.M. Sparlin, S.R. Sehlin, Solid State Ionics 76 (1995) 259–271.
[9] L.W. Tai, M.M. Nasrallah, H.U. Anderson, D.M. Sparlin, S.R. Sehlin, Solid State Ionics 76 (1995) 273–283.
[10] B.T. Dalselet, M. Søgaard, H.J.M. Bouwmeester, P.V. Hendriksen, Solid State Ionics 180 (2009) 1173–1182.
[11] Y. Teraoka, S. Furukawa, H.M. Zhang, N. Yamazoe, J. Chem. Soc. Jpn. 7 (1988) 1084–1089.
[12] T. Ishihara, K. Nakashima, S. Okada, M. Enoki, H. Matsumoto, Solid State Ionics 179 (2008) 1367–1371.
[13] M.-B. Choi, S.-Y. Jeon, J.-Y. Park, H.-S. Yang, S.-J. Song, Solid State Ionics 192 (2011) 269–274.
[14] M.-B. Choi, D.-K. Lim, E.D. Wachsman, S.-J. Song, Solid State Ionics 221 (2012) 22–27.
[15] J.-S. Ahn, S. Omar, H.-S. Yoon, J.C. Nino, E.D. Wachsman, J. Power Sources 195 (2010) 2131–2135.
[16] J.-S. Ahn, H.-S. Yoon, K.-T. Lee, M.A. Camaratta, E.D. Wachsman, Fuel Cells 9 (2009) 643–649.
[17] K.-T. Lee, D.-W. Jung, M.A. Camaratta, H.-S. Yoon, J.-S. Ahn, E.D. Wachsman, J. Power Sources 205 (2012) 122–128.
[18] C.-R. Song, H.-I. Yoo, Phys. Rev. B 616 (2000) 3975–3982.
[19] C.J. Reidy, T.J. Fleming, M.R. Towler, S. Hampshire, Int. J. Appl. Ceram. Technol. 8 (2011) 1475–1485.
[20] H.-I. Yoo, S.-H. Park, J. Chun, J. Electrochemical Soc. 157 (2010) B215–B219.